

# Continuum Percolation Thresholds in Two Dimensions

Stephan Mertens  
Christopher Moore

SFI WORKING PAPER: 2012-09-016

SFI Working Papers contain accounts of scientific work of the author(s) and do not necessarily represent the views of the Santa Fe Institute. We accept papers intended for publication in peer-reviewed journals or proceedings volumes, but not papers that have already appeared in print. Except for papers by our external faculty, papers must be based on work done at SFI, inspired by an invited visit to or collaboration at SFI, or funded by an SFI grant.

©NOTICE: This working paper is included by permission of the contributing author(s) as a means to ensure timely distribution of the scholarly and technical work on a non-commercial basis. Copyright and all rights therein are maintained by the author(s). It is understood that all persons copying this information will adhere to the terms and constraints invoked by each author's copyright. These works may be reposted only with the explicit permission of the copyright holder.

[www.santafe.edu](http://www.santafe.edu)



SANTA FE INSTITUTE

# Continuum Percolation Thresholds in Two Dimensions

Stephan Mertens<sup>1,2,\*</sup> and Cristopher Moore<sup>1,†</sup>

<sup>1</sup>*Santa Fe Institute, 1399 Hyde Park Rd., Santa Fe, NM 87501, USA*

<sup>2</sup>*Institut für Theoretische Physik, Universität Magdeburg, Universitätsplatz 2, 39016 Magdeburg, Germany*

(Dated: September 25, 2012)

A wide variety of methods have been used to compute percolation thresholds. In lattice percolation, the most powerful of these methods consists of microcanonical simulations using the union-find algorithm to efficiently determine the connected clusters, and (in two dimensions) using exact values from conformal field theory for the probability, at the phase transition, that various kinds of wrapping clusters exist on the torus. We apply this approach to percolation in continuum models, finding overlaps between objects with real-valued positions and orientations. In particular, we find new values of the percolation transition for disks, squares, rotated squares, and rotated sticks in two dimensions, and confirm that these transitions behave as conformal field theory predicts. The running time and memory use of our algorithm are essentially linear as a function of the number of objects at criticality.

What happens to the hole when the cheese is gone?

Bertold Brecht, *Mother Courage*

## I. INTRODUCTION

For more than 50 years, percolation theory has been used to model static and dynamic properties of porous media and other disordered physical systems [1–3]. Most natural systems correspond to continuum percolation, yet most analytical and numerical work has focused on lattice percolation. This is reasonable since continuum and lattice percolation lie in the same universality class. For properties that are non-universal, however, such as the location of the threshold, one has to study discrete and continuum models individually, and it is also satisfying to confirm universality experimentally by measuring critical exponents and crossing probabilities.

In this contribution we discuss an algorithm to compute the location of the transition in continuum percolation models. The algorithm works in arbitrary dimensions, and for arbitrarily shaped objects; here we focus on two-dimensional percolation with disks, squares that are aligned or randomly rotated, and randomly rotated sticks (see Figure 1). Our algorithm is an adaption of the union-find algorithm of Newman and Ziff [4], the fastest known algorithm for lattice percolation. We show that it can be adapted to continuum percolation with the aid of some simple additional data structures, and we back up our claim by computing numerical values of the transition points that extend the accuracy of previously known values by several orders of magnitude.

In two-dimensional continuum percolation, a number  $n$  of penetrable objects are thrown at random in a square of size  $L^2$ . If the mean density  $\rho = n/L^2$  is finite as  $n$  and

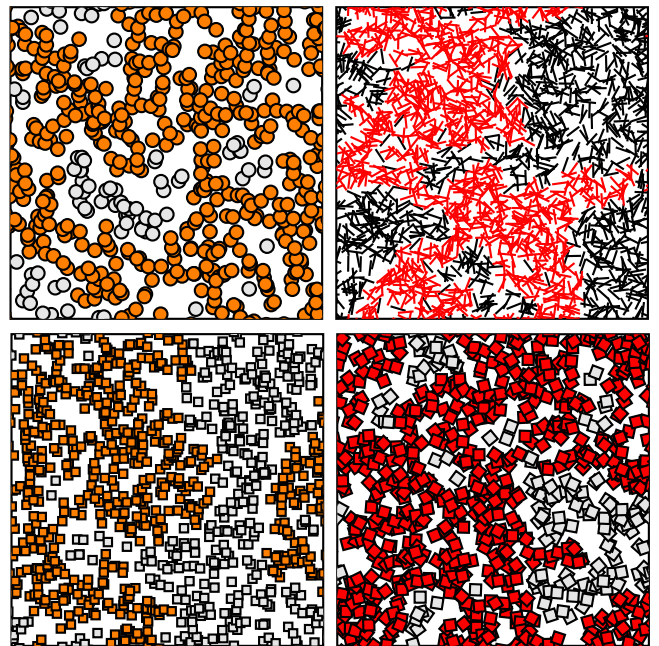


Figure 1. Continuum percolation with disks, randomly rotated sticks, and aligned or rotated squares. In each example, the wrapping cluster is marked by color.

$L$  go to infinity, the spatial distribution of the objects' centers is a Poisson point process with density  $\rho$ . The system percolates if there exists a cluster of overlapping objects that spans the square. We follow [4] in using periodic boundary conditions, and focusing on clusters that wrap around horizontally, vertically, or both. These wrapping clusters display better finite-size effects than crossing clusters on open boundary conditions.

If each object has area  $a$ , then the probability that a percolating cluster exists in the limit  $L \rightarrow \infty$  clearly depends only on the product  $\eta = \rho a$ . This dimensionless quantity is called the *filling factor*. It also gives the total fraction  $\phi$  of the plane covered by the objects,

$$\phi = 1 - e^{-\eta}. \quad (1)$$

\* mertens@ovgu.de

† moore@santafe.edu

While we expect continuum percolation to be in the same universality class for any fixed shape, the location of the transition, i.e., the critical filling factor  $\eta_c$ , depends on the shape of the objects. We write  $\eta_c^\circ$ ,  $\eta_c^\square$ ,  $\eta_c^\diamond$ , and  $\eta_c^\times$  for the percolation of disks, aligned squares, randomly rotated squares, and randomly rotated sticks. In defining  $\eta$ , we treat sticks of length  $\ell$  as if they have area  $a = \ell^2$ .

Table I lists the most accurate numerical values for  $\eta_c$  from previous work and the work presented here. The best previous results on disk percolation are due to Quintanilla, Torquato, and Ziff [5] who varied the density of the Poisson process as a function of position and kept track of the front of the connected cluster. The best previous results on aligned squares are due to Torquato and Jaio [7], who rescale an initial set of particles so that its density is close to rigorous bounds. The best previous results on rotated squares are due to Baker et al. [6]. The best previous results on sticks are due to Li and Zhang [8], who used an approach similar to ours but with open boundary conditions.

Our results are consistent with the rigorous bounds

$$\begin{aligned} 1.127 &\leq \eta_c^\circ \leq 1.12875 \\ 1.098 &\leq \eta_c^\square \leq 1.0995, \end{aligned} \quad (2)$$

computed with 99.99% confidence by Balister, Bollobás and Walters [9] using a Monte Carlo estimate of a high-dimensional integral. On the other hand, it is a little sad to dash the hope—which one might have entertained after reading [6, 7], and which is just barely consistent with (2)—that  $\phi_c^\square$  is exactly  $2/3$ .

In the following sections, we review the union-find algorithm of [4], how it finds wrapping clusters in periodic boundary conditions, and how we extend it to the continuous case. We show that the running time of our algorithm is essentially linear in the number of objects, i.e., linear in  $L^2$ . In addition to estimating the threshold, we also measure the finite-size exponent  $\nu$ , giving strong evidence that these continuum models are in the same universality class as lattice percolation. Finally, we find that the probability of a wrapping cluster at criticality is precisely that predicted by conformal field theory.

## II. THE ALGORITHM

We will simulate percolation in the microcanonical ensemble, i.e., where the number  $n$  of objects in the square is fixed. In each trial, we add one object at a time, stopping as soon as a percolating cluster appears. Following [4], we keep track of the connected components at each step using the union-find data structure. In union-find, each cluster is represented uniquely by one of its members. We have access to two functions:  $\text{find}(i)$ , which finds the representative  $r(i)$  of the cluster to which object  $i$  belongs, and  $\text{merge}(i, j)$ , which merges  $i$ 's cluster and  $j$ 's cluster together into a single one with the same representative.

Internally, union-find works in a very simple way. Each object  $i$  is linked to a unique “parent”  $p(i)$  in the

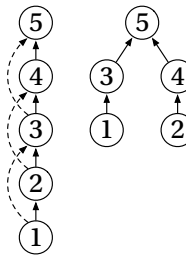


Figure 2. When we call  $\text{find}(i)$ , we split and shorten the path from  $i$  to its representative  $r(i)$  by setting the parent of each object along the path to be its grandparent. This turns a path of length  $\ell$  into two paths of length  $\ell/2$ .

same cluster, except for the representative which has no parent. When we call  $\text{find}(i)$ , it follows the links from  $i$  to its parent  $p(i)$ , its grandparent  $p(p(i))$ , and so on, until it reaches  $i$ 's representative  $r(i)$ . Similarly,  $\text{merge}(i, j)$  uses  $\text{find}(i)$  and  $\text{find}(j)$  to obtain  $r(i)$  and  $r(j)$ , and declares one of them to be the parent of the other, unless  $r(i) = r(j)$  and they are already in the same cluster.

The running time of  $\text{find}(i)$  is proportional to the length of the path from  $i$  to  $r(i)$ . If  $\text{merge}(i, j)$  sensibly links the smaller cluster to the larger one, setting  $p(r(i)) = r(j)$  whenever  $i$ 's cluster is smaller than  $j$ 's, a simple inductive argument shows that these paths never exceed  $\log_2 n$  in length. However, we can make these paths even shorter using a trick called *path compression*. Since  $r(i)$  is the representative of every object  $j$  along the path from  $i$  to  $r(i)$ , we can set  $p(j) = r(i)$  for all of them, linking them directly to their representative so that  $\text{find}$  will work in a single step the next time we call it.

As a result, the *amortized cost* of the  $\text{find}$  and  $\text{merge}$  operations—that is, the average cost per operation over the course of many operations—is nearly constant. Specifically, it is proportional to  $\alpha(n)$ , when  $\alpha$  is the inverse of the Ackermann function [10]. The Ackermann function grows faster than any primitive recursive function, i.e., any function that can be computed with a fixed number of for-loops: faster than an exponential, an iterated tower of exponentials, and so on [11]. As a consequence,  $\alpha(n)$  grows incredibly slowly, and the smallest value of  $n$  such that  $\alpha(n) > 4$  is so large that it can only be written with exotic notation. Thus the total running time for  $n$  objects is essentially  $O(n)$ .

In our implementation, we employ a form of path compression that is faster and almost as effective: we link each object  $j$  on the path to its grandparent, setting  $p(j) = p(p(j))$ . This is known as *path splitting*, since it turns a path of length  $\ell$  into two paths of length  $\ell/2$ , or  $(\ell + 1)/2$  and  $(\ell - 1)/2$  if  $\ell$  is odd, as shown in Figure 2. It has the advantage of requiring only one pass along the path, and it takes just one line of code (e.g. [4, Appendix A]). Like path compression, it guarantees an amortized running time of  $O(\alpha(n))$  [12].

For lattice percolation as in [4], each time we add a

	$\eta_c^\circ$	$\eta_c^\square$	$\eta_c^\diamond$	$\eta_c^\times$
previous	1.128085(2)	1.0982(3)	0.9819(6)	5.63726(2)
our work	1.12808737(6)	1.09884280(9)	0.9822723(2)	5.6372858(6)
	$\phi_c^\circ$	$\phi_c^\square$	$\phi_c^\diamond$	$\phi_c^\times$
previous	0.6763475(6)	0.6665(1)	0.6254(2)	0.99643738(7)
our work	0.67634831(2)	0.66674349(3)	0.62554075(8)	0.996437475(2)

Table I. Numerical values of critical filling factors  $\eta_c$  and area factors  $\phi_c = 1 - e^{-\eta_c}$  in continuum percolation for disks, aligned squares, randomly rotated squares, and randomly rotated sticks. Previous estimates are from [5–8].

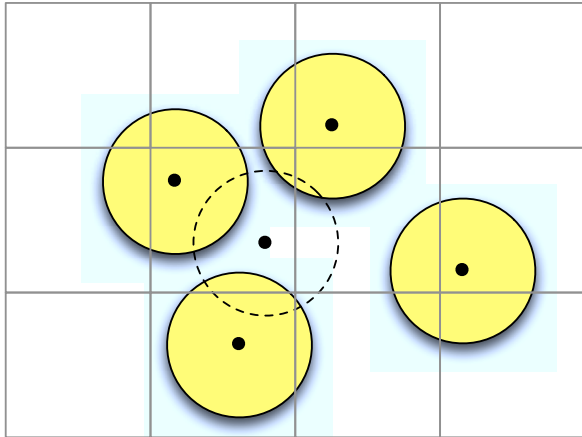


Figure 3. We divide the plane into square bins whose width equals the diameter of the disks. Each disk in a given bin (dashed) can only intersect with other disks in the same bin, or in the eight neighboring bins.

new occupied site, we can check which of its neighbors are occupied, and merge them together with the new site. In the continuous case, we have more work to do: if we add a new disk (say), we have to find which nearby disks it intersects. To do this efficiently, we divide the plane into square bins as shown in Figure 3. Each disk belongs to whichever bin its center lies in. The width of each bin is the diameter of the disks, so that a disk in a given bin can only intersect with other disks in that bin or the eight bins in its neighborhood.

On average, the number of disks in each bin is a constant proportional to  $\rho$ , so we can find all the disks intersecting with each new one in constant time. We use the same approach for the other shapes; for rotated squares of width  $\ell$ , the bins need to have width  $\sqrt{2}\ell$ . A similar approach for rotated sticks was used in [8].

If we wished to detect crossing clusters—those that connect, say, the top and bottom edges of the square—we could add two special objects to the union-find data structure, which are connected by fiat to all the disks in the bins along the top or bottom edge. We would then check, at each step, whether these two objects are in the same cluster. However, as discussed below and in [4], the finite-size scaling is much better if we use periodic boundary conditions instead, and look for clusters that

wrap around the torus horizontally or vertically.

We detect these wrapping clusters using a technique originally used for detecting crossing clusters in the Potts model [13]. We associate a vector with each object in the union-find data structure, recording the displacement between it and its parent. In principle this displacement is real-valued, but it suffices to record an integer vector giving the displacement between their respective bins. When we compress and splint a path, we sum these vectors to get the total displacement between each object on the path and its new parent.

Now suppose that  $\text{merge}(i, j)$  finds that two overlapping disks  $i$  and  $j$  are already in the same cluster. Object  $i$  now has two paths to its representative; one that goes through its own parent, and another that consists of hopping to  $j$  and then going through  $j$ 's parents. We sum the displacement vectors along both these paths. If these sums are the same, then the cluster is simply-connected. But if they differ by  $\pm L$  in either coordinate, then the cluster has a nontrivial winding number around one or both directions on the torus.

Like the union-find algorithm itself, the time it takes to sum these vectors is proportional to the length of the paths from  $i$  and  $j$  to their representative. As Figure 4 shows, the total running time of our entire algorithm—the time it takes to carry out a trial on a lattice of size  $L$ , adding objects one at a time until a wrapping cluster appears—is essentially linear in the number  $n$  of objects at criticality, or equivalently linear in  $L^2$ . It slows down somewhat when the computer is forced to switch to parts of its memory with slower access, but this only affects the leading constant.

### III. ANALYSIS AND RESULTS

If in each trial we stop at the first  $n$  where a wrapping cluster appears, then the estimated probability  $P_L(a, n)$  that a wrapping cluster exists in the microcanonical ensemble with  $n$  objects of area  $a$  is the fraction of trials that stop on or before the  $n$ th step. To obtain the probability  $R_L(\eta)$  of percolation in the grand canonical ensemble with filling fraction  $\eta$ , we convolve  $P_L$  with the Poisson distribution with mean  $\lambda = \rho L^2 = \eta L^2/a$ :

$$R_L(\eta) = e^{-\lambda} \sum_{n=0}^{\infty} \frac{\lambda^n}{n!} P_L(a, n). \quad (3)$$

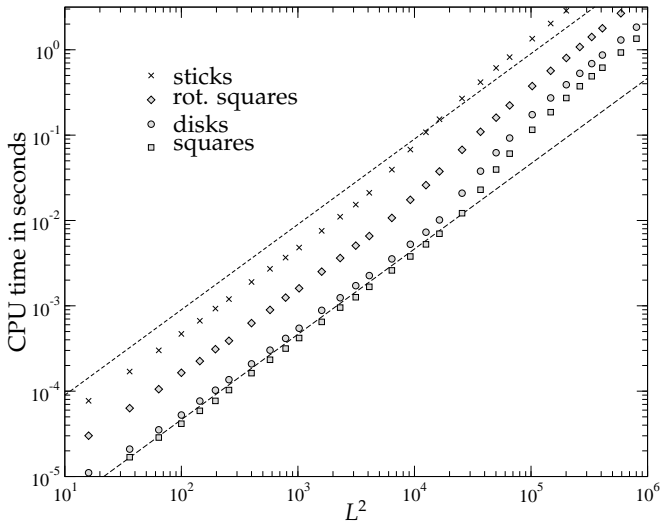


Figure 4. Average CPU time  $T$  for a single realization of an  $L \times L$  lattice up to the percolation transition.  $T$  is measured on a laptop with Intel Core 2 Duo 2.53 GHz CPU with 3 MB cache. The dashed lines  $T \propto L^2$  are guides for the eye. The slope increases when the cache memory is exhausted, forcing the computer to switch to regions of memory with slower access; however, the running time remains linear in  $n \propto L^2$ .

To avoid numerical difficulties where the numerator and denominator are both very large, we compute Poisson weights  $w_n \propto \lambda^n/n!$  inductively in two sequences  $w_{\bar{n}-k}$  and  $w_{\bar{n}+k}$  to the left and right of the peak at  $\bar{n} = \lfloor \lambda \rfloor$ , where we define  $w_{\bar{n}} = 1$ :

$$w_{\bar{n}-k} = \begin{cases} 1 & \text{for } k = 0 \\ \frac{\lambda}{\bar{n}-(k-1)} w_{\bar{n}-(k-1)} & \text{for } k = 1, 2, \dots \end{cases}$$

and

$$w_{\bar{n}+k} = \begin{cases} 1 & \text{for } k = 0 \\ \frac{\lambda}{\bar{n}+k} w_{\bar{n}+k-1} & \text{for } k = 1, 2, \dots \end{cases}$$

The sum (3) only needs to be computed for a finite number of terms. In one direction, we only need to sum down to the smallest  $n$  where  $P_L(a, n)$  is nonzero, i.e., the smallest value of  $n$  where we observed a wrapping cluster in at least one trial. In the other direction, once we pass the largest  $n$  where a wrapping cluster first appeared, then  $P_L(a, n) = 1$ . At that point, we sum the remaining terms until they are zero to within the numerical precision of the computer. We then normalize the entire sum by dividing by  $\sum w_n$ .

Equipped with the data from the microcanonical simulations and this convolution routine, we compute the wrapping probability functions  $R_L(\eta)$  for various system sizes  $L$  and shapes. Like [4], we look for several kinds of wrapping in particular. Specifically:

- $R_L^e(\eta)$  is the probability of any kind of wrapping cluster. This is indicated by a winding number that is nonzero in either coordinate.

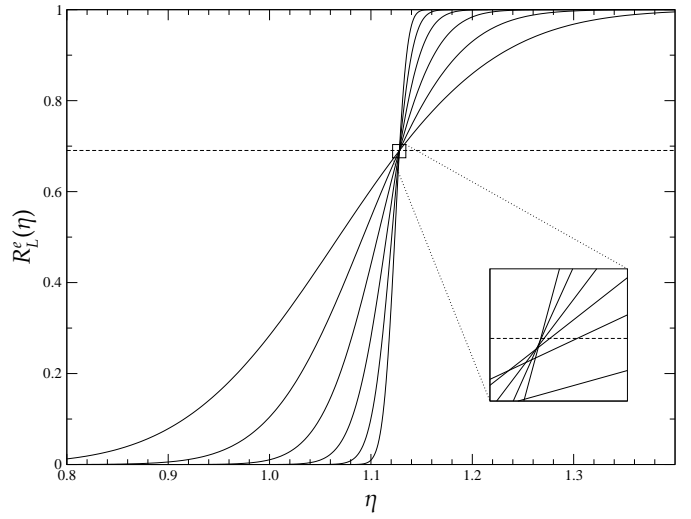


Figure 5. Wrapping probabilities  $R_L^e(\eta)$  for disk percolation and  $L = 16, 32, 64, 128, 256, 512$ . The dashed line is the exact value of the critical wrapping probability  $R_\infty^e(\eta_c)$  from conformal field theory.

- $R_L^h(\eta)$  is the probability of a cluster that wraps horizontally. This is indicated by a winding number that is nonzero in the first coordinate.
- $R_L^b(\eta)$  is the probability of a cluster that wraps both horizontally and vertically. This is indicated by a single winding number that is nonzero in both coordinates, or a pair of winding numbers that are nonzero in the first and second coordinates respectively.
- $R_L^1(\eta)$  is the probability of a cluster that wraps horizontally, both not vertically. This is indicated by a winding number that is nonzero in only the first coordinate.

For any  $L$  and any  $\eta$ , these probabilities obey

$$R_L^e = 2R_L^h - R_L^b = 2R_L^1 + R_L^b.$$

We assume here that the torus is square, so that horizontal and vertical wrapping probabilities are equal.

Note that if the first nonzero winding number observed in a given trial is nonzero in both coordinates, then a cluster of type 1 (horizontal but not vertical) does not occur at all in that trial. Thus  $R_L^1(\eta)$  does not tend to 1 as  $\eta$  increases.

In practice, we focused on  $R_L^e$  and  $R_L^b$ . In each run, we recorded the number of objects  $n^h$  at which horizontal wrapping first occurred, and the number  $n^v$  at which vertical wrapping first occurred. Then  $n^e = \min(n^h, n^v)$  and  $n^b = \max(n^h, n^v)$  are our estimates, in that run, of the values of  $n$  at which  $R_L^e$  and  $R_L^b$  jump from 0 to 1.

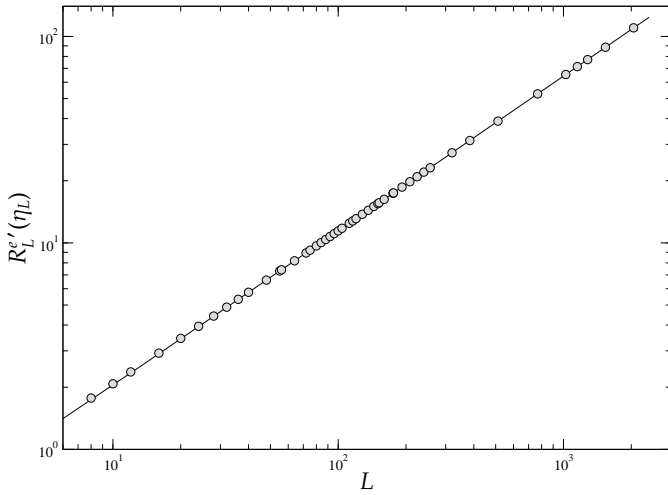


Figure 6. Slope of  $R_L^e(\eta)$  at  $\eta_L$ , the estimated critical filling factor. The line is  $0.361L^{3/4}$ , confirming the universal critical exponent  $\nu = 4/3$  for finite-size scaling.

A beautiful fact is that, even though the percolation threshold  $\eta_c$  is not known for any of our models, conformal field theory implies exact values for these probabilities at the transition in the limit  $L \rightarrow \infty$  [4, 14]. Specifically,

$$\begin{aligned} R_\infty^h &= 0.521\,058\,289\,248\,821\,787\,848\dots \\ R_\infty^e &= 0.690\,473\,724\,570\,168\,677\,230\dots \\ R_\infty^b &= 0.351\,642\,853\,927\,474\,898\,465\dots \\ R_\infty^1 &= 0.169\,415\,435\,321\,346\,889\,383\dots \end{aligned} \quad (4)$$

For each  $L$ , and each type of wrapping cluster, we can estimate the critical filling factor  $\eta_L$  as the solution of the equation

$$R_L(\eta_L) = R_\infty. \quad (5)$$

For instance, Figure 5 shows  $R_L^e(\eta)$  for disks for  $L$  ranging up to 512. The filling factors  $\eta_L$  where these curves cross  $R_\infty^e$  rapidly converge to  $\eta_c$ .

The rate of convergence is determined by two factors. The first comes from the fact that the width of the transition window from  $R_L \approx 0$  to  $R_L \approx 1$  scales as  $L^{-1/\nu}$  where  $\nu = 4/3$  is a universal critical exponent for two-dimensional percolation. This scaling holds even for small systems, as can be seen in Figure 6, where we plot the slope of  $R_L$  at the estimated critical filling factor  $\eta_L$ . The slope scales perfectly like  $L^{3/4}$ .

The second factor comes from the fact that  $R_L(\eta)$  not only becomes steeper but also moves upward in the critical region (see the inset in Figure 5). To measure the contribution from this effect, we computed the difference  $R_L(\eta_c) - R_\infty^e$  using the previously best known value for  $\eta_c$  from Table I. This difference scales like  $L^{-2}$ , as can be seen from Figure 7. The same scaling has been observed

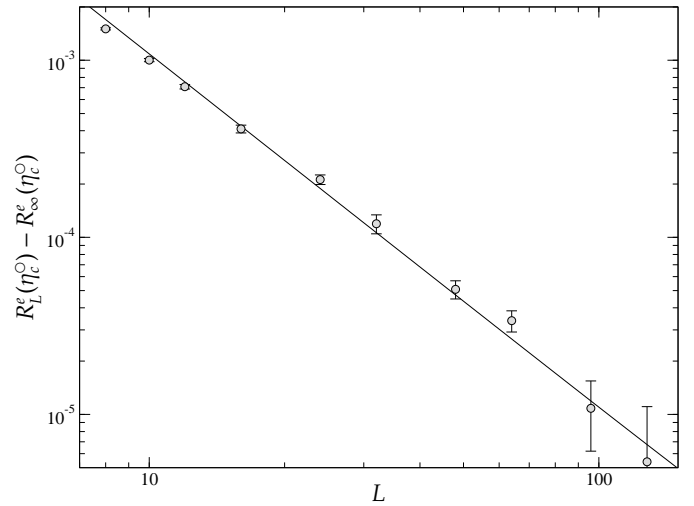


Figure 7. Convergence with increasing system size  $L$  of  $R_L^e(\eta_c)$  to its known value at  $L = \infty$  for disk percolation. The line is proportional to  $L^{-2}$ , the conjectured convergence of  $R_L^e(\eta_c)$ .

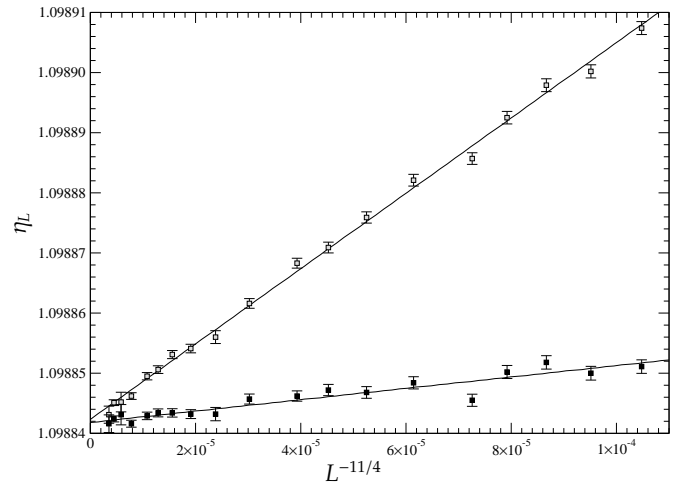


Figure 8. Estimated critical filling factors for continuum percolation of squares, derived from (5) with  $R_L^e$  (top) and  $R_L^b$  (bottom). Note the resolution of the  $\eta$ -axis.

in two-dimensional lattice percolation [4]. Note that the periodic boundary conditions are responsible for this quadratic decay. With open boundary conditions, this factor scales as  $L^{-1}$  [15], leading to more severe finite-size effects.

These two factors combine to give

$$\eta_L - \eta_c \sim L^{-2-1/\nu} = L^{-11/4} \quad (6)$$

for the rate of convergence. Hence we expect a straight line if we plot  $\eta_L$  vs.  $L^{-11/4}$ , and this is exactly what we observe in Figure 8. Extrapolating this line to zero then gives our estimates of  $\eta_c$  shown in Table I.

How do we compute the error bars in our estimates of  $\eta_c$ ? First consider the fluctuations in  $R_L(\eta)$ . Each of our microcanonical experiments contributes to our estimate of  $R_L(\eta)$  for all  $\eta$  through the convolution (3). We can imagine this as choosing  $n$  from the Poisson distribution, adding  $n$  objects, and returning an estimate of  $R_L(\eta) = 1$  or 0 depending on whether they percolate or not. If we perform  $N$  trials, the number of trials that return 1 is binomially distributed with mean  $R_L(\eta)N$ , and averaging gives an estimate of  $R_L(\eta)$  with standard deviation

$$\sigma_{R_L} = \sqrt{\frac{R_L(\eta)(1 - R_L(\eta))}{N}}. \quad (7)$$

Depending on which kind of wrapping cluster we are looking for, this is roughly  $0.4N^{-1/2}$ .

When we look for the  $\eta_L$  where  $R_L(\eta)$  crosses  $R_\infty$ , the error on  $\eta_L$  is given by

$$\sigma_{\eta_L} = \frac{\sigma_{R_L}}{R'_L(\eta_L)}.$$

Since the slope  $R'_L(\eta_L)$  grows as  $0.361L^{3/4}$  (see Figure 6) this gives

$$\sigma_{\eta_L} \approx N^{-1/2} L^{-3/4}.$$

These are the error bars shown in Figure 8.

The extrapolated value for  $\eta_c$  is computed from simulations for  $D$  different system sizes  $L$ , which in a weighted linear regression as in Figure 8 yields an error roughly  $\sqrt{D}$  times smaller than the error bars of the underlying data points.

Finally, we average our estimates of  $\eta_c$  from  $R_L^e$  and  $R_L^b$ . Assuming that these estimates are only weakly correlated reduces the error bars by another factor of  $\sqrt{2}$ .

The error bars shown in Table I are the result of simulating roughly  $D = 50$  system sizes ranging from  $L = 8$  to  $L = 2048$ , with sample sizes  $N$  ranging from  $10^{10}$  for the systems with  $L \leq 100$ , to  $10^9$  for  $100 < L \leq 500$ , to  $10^6$  for  $500 < L \leq 2048$ .

We ran these simulations in parallel on several computer clusters with greatly varying computational power. In total, our simulations would have taken about 400 years if done only on the laptop on which this paper was written.

#### IV. CONCLUSIONS

We have shown that the union-find approach to estimating percolation thresholds introduced by Newman and Ziff [4] can be applied in the continuous case. With the help of an algorithm for estimating  $\eta_c$  that runs in essentially linear time as a function of the number of objects at criticality, we have obtained new estimates for  $\eta_c$  in a variety of continuum percolation models that are several orders of magnitude more accurate than previous results. In the process, we have confirmed the predictions of conformal field theory for these models, both for the finite-size scaling exponent  $\nu$  and the probabilities that various kinds of wrapping clusters exist at  $\eta_c$  on periodic boundary conditions.

#### ACKNOWLEDGMENTS

S.M. thanks the Santa Fe Institute for their hospitality. C.M. is supported by the National Science Foundation through grant CCF-1219117 and by the Air Force Office of Scientific Research and the Defense Advanced Research Projects Agency through grant FA9550-12-1-0432. We are grateful to Robert Ziff and Mark Newman for helpful conversations.

- 
- [1] E. N. Gilbert, *Journal of the Society for Industrial and Applied Mathematics* **9**, 533 (1961).
  - [2] D. Stauffer and A. Aharony, *Introduction to Percolation Theory* (Taylor & Francis, London, 1992).
  - [3] M. Sahimi, *Applications of Percolation Theory* (Taylor & Francis, London, 1994).
  - [4] M. E. J. Newman and R. M. Ziff, *Physical Review E* **64**, 016706 (2001).
  - [5] J. A. Quintanilla and R. M. Ziff, *Physical Review E* **76**, 051115 (2007).
  - [6] D. R. Baker, G. Paul, S. Sreenivasan, and H. E. Stanley, *Physical Review E* **66**, 046136 (2002).
  - [7] S. Torquato and Y. Jiao, *Journal of Chemical Physics* **137**, 074106 (2012).
  - [8] J. Li and S.-L. Zhang, *Physical Review E* **80**, 040104(R) (2009).
  - [9] P. Balister, B. Bollobás, and M. Walters, *Random Structures & Algorithms* **26**, 392 (2005).
  - [10] R. E. Tarjan, *Journal of the Association for Computing Machinery* **22**, 215 (1975).
  - [11] C. Moore and S. Mertens, *The Nature of Computation* (Oxford University Press, 2011) [www.nature-of-computation.org](http://www.nature-of-computation.org).
  - [12] R. E. Tarjan and J. van Leeuwen, *Journal of the Association for Computing Machinery* **31**, 245 (1984).
  - [13] J. Machta, Y. S. Choi, A. Lucke, T. Schweizer, and L. M. Chayes, *Physical Review E* **54**, 1332 (96).
  - [14] H. T. Pinson, *Journal of Statistical Physics* **75**, 1167 (1994).
  - [15] J.-P. Hovi and A. Aharony, *Physical Review E* **53**, 235 (1996).